AIAA JOURNAL
Vol. 32, No. 5, May 1994

Repeatability and Uncertainty Analyses of Light Gas Gun Test Data

William P. Schonberg* and David Cooper†
University of Alabama in Huntsville, Huntsville, Alabama 35899

All large spacecraft are susceptible to high-speed impacts by meteoroids and pieces of orbiting space debris which can damage flight-critical systems and in turn lead to catastrophic failure. One way to obtain information on the response of a structure to a meteoroid impact or an orbital debris impact is to simulate the impact conditions of interest in the laboratory and analyze the resulting damage to a target structure. As part of the Phase B and C/D development activities for the Space Station Freedom, 950 impact tests were performed using the NASA/Marshall Space Flight Center (MSFC) light gas gun from 1985–1991. This paper presents the results of impact phenomena repeatability and data uncertainty studies performed using the information obtained from those tests. The results of these studies can be used to assess the utility of individual current and future NASA/MSFC impact test results in the design of long-duration spacecraft.

I. Introduction

ALL large spacecraft are susceptible to impacts by meteoroids and pieces of orbiting space debris. These impacts occur at extremely high speeds and can damage flight-critical systems, which can in turn lead to catastrophic failure of the spacecraft. The susceptibility of a spacecraft to such impacts increases with increased mission duration. Therefore, the design of a spacecraft for a long-duration mission must take into account the possibility of these hypervelocity impacts and their effects on the spacecraft structure and on all of its exposed subsystem components. One way to obtain information on the response of a structure to a meteoroid impact or an orbital debris impact is to subject a target structure to simulated impact conditions of interest and analyze the resulting damage to a target structure.

High-speed impact testing was first performed at the NASA/Marshall Space Flight Center (MSFC) in 1964 with the installation of a light gas gun in what is now known as the Materials and Processes Laboratory. The NASA/MSFC hypervelocity impact test facility consists of an instrumented two-stage light gas gun capable of launching 2.5–12.7-mm-diam projectiles at velocities of 2–8 km/s. Projectile velocity measurements are done using pulsed x-ray, laser diode detectors, and a Hall photographic station.[1] The initial need and function of the facility was to provide a means of simulating meteoroid impacts on spacecraft and to provide the data required to determine the perforation probability of candidate spacecraft wall designs by such impacts. In the 1970's, the interest in testing for protection against meteoroid impacts declined. However, the increased spacecraft launch activity in recent years has renewed interest in high-speed impact testing at the NASA/MSFC facility and at other such facilities around the world. The attention of this new wave of testing has been focused on mitigating the threat posed by impacts due to orbital debris.

II. Hypervelocity Impact Testing at NASA/Marshall Space Flight Center

Orbital debris impact testing began at NASA/MSFC in 1985 as part of the Space Station Freedom design and development activities. As part of the Phase B development activities, 540 impact tests were performed using the NASA/MSFC light gas gun from July 1985–March 1989; an additional 410 tests were performed as part of the Phase C/D activities through February 1991. Testing has been focused primarily on multiwall target structures that were designed to simulate possible Space Station module wall configurations. These target systems consisted of bumper, pressure wall, and witness plates and multilayer thermal insulation (MLI). An illustration of a typical dual-wall structure undergoing normal high-speed impact is shown in Fig. 1. In this figure, t_s and t_w are the thickness of the bumper and pressure wall plates, respectively, S is the bumper-to-pressure-wall spacing (i.e., the stand-off distance in a dual-wall system), and D, θ, and V are the projectile diameter, impact trajectory, and impact velocity, respectively.

In the impact tests performed, aluminum projectiles ranging in diameter from 3.175 mm to 9.53 mm were fired towards the target structure at velocities ranging from approximately 2 to 8 km/s. The target structures consisted primarily of aluminum plates of various thicknesses and spaced apart at various dis-

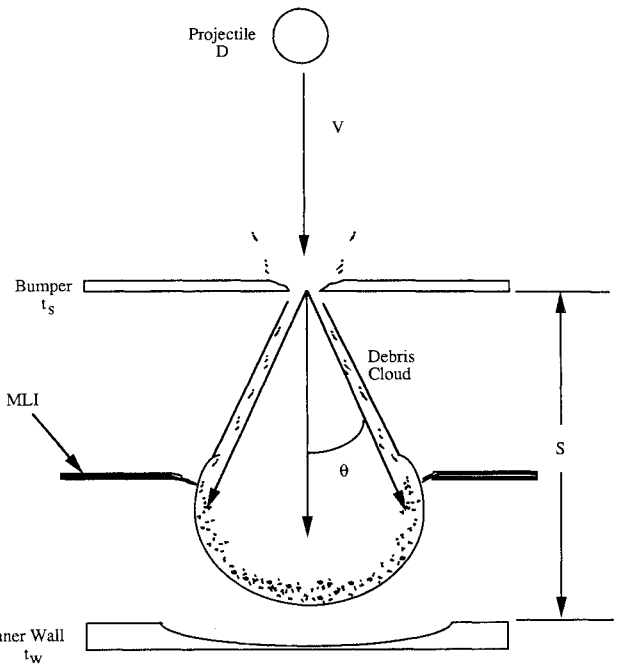

Fig. 1 Response of a dual-wall structure to a hypervelocity impact.

Received May 28, 1993; revision received Oct. 15, 1993; accepted for publication Nov. 5, 1993.

*Associate Professor, Civil and Environmental Engineering Department. Member AIAA.

†Graduate Research Assistant, Mechanical and Aerospace Engineering Department.

tances. Tests were performed without and with MLI blankets of various thicknesses placed at various positions within the spacing between the bumper plate and the pressure wall plate in the test specimens. Although a majority of the testing was performed with impacts normal to the plane of the target, a significant number of oblique impact tests was performed as well. A complete list of the Phase B and C/D test parameters as well as results from various damage analyses performed can be found in Refs. 2 and 3. An overall summary of the Phase B and Phase C/D test parameters is presented in Table 1 where tests are grouped into broad categories such as impact velocity, projectile diameter, impact obliquity, configuration, and stand-off distance.

III. Objectives and Methodology Overview

This paper presents results of impact phenomena repeatability and data uncertainty studies performed using information obtained from impact tests performed at NASA/MSFC between 1985 and 1991. The objectives of the analyses were two-fold: first, to quantify the repeatability of the phenomena ocurring in dual-wall structures under hypervelocity impact based on the testing performed at the NASA/MSFC light gas gun during the time period 1985–1991, and, second, to determine the uncertainty of the measurements taken from the damaged test specimens. The results of these analyses can be used to assess the utility of individual current and future NASA/MSFC impact test results in the design of long-duration spacecraft.

Table 1 Summary of tests performed at NASA/Marshall Space Flight Center from 1985 to 1991

		Phase B	Phase C/D	Combined
Velocity (km/s)	$7.0 \le V < 8.0^{+}$	61	60	121 (12.7%)
	$6.0 \le V < 7.0$	165	137	302 (31.8%)
	$5.0 \le V < 6.0$	94	82	176 (18.5%)
	$4.0 \le V < 5.0$	103	57	160 (16.8%)
	$3.0 \le V < 4.0$	85	60	145 (15.3%)
	$2.0 \le V < 3.0$	31	14	45 (4.8%)
	$1.0 \le V < 2.0$	1	0	1 (0.1%)
		540	410	950 (100%)
Diameter (cm)	$1.00 \le D \le 1.25$	16	12	28 (2.9%)
	$0.75 \le D < 1.00$	218	173	391 (41.1%)
	$0.50 \le D < 0.75$	200	137	337 (35.5%)
	$0.25 \le D < 0.50$	106	88	194 (20.5%)
		540	410	950 (100%)
Obliquity (deg)	0	337	207	544 (57.3%)
	15	1	0	1 (0.1%)
	25	1	0	1 (0.1%)
	30	11	11	22 (2.3%)
	45	128	99	227 (23.8%)
	55	3	0	3 (0.3%)
	60	10	40	40 (5.3%)
	65	44	20	64 (6.7%)
	75	5	33	38 (4.1%)
		540	410	950 (100%)
Configuration	Single wall	11	0	11 (1.1%)
	1 Bumper	396	392	788 (82.9%)
	2 Bumpers	89	13	102 (10.7%)
	3 Bumpers	6	5	11 (1.1%)
	4 Bumpers	3	0	3 (0.3%)
	6 Bumpers	1	1	1 (0.1%)
	Windows	26	0	26 (2.8%)
	Bottles	8	8	8 (1.0%)
		540	410	950 (100%)
Stand-off distance (cm) (Single bumper)	10.16	334	333	667 (84.6%)
	15.24	52	11	63 (8.0%)
	17.78	1	0	1 (0.1%)
	20.32	3	0	3 (0.3%)
	30.48	5	48	53 (6.8%)
	40.64	1	0	1 (0.1%)
		396	410	950 (100%)

The objective of the first stage of the analysis was to determine whether identical dual-wall structures would be perforated or exhibit rear-side spallation for the same impact conditions. At issue was only the consistency in the test results for overall structural response—perforation vs no perforation or spall vs no spall—under the same impact conditions. Because no measureable quantity was involved in this stage of the analysis, standard uncertainty analysis procedures (see, e.g., Ref. 4) were not used; only an approximate quantifiable measure of the overall repeatability of the phenomena ocurring in dual-wall structures under hypervelocity impact based on testing at the NASA/MSFC light gas gun facility was obtained.

The second stage of the analysis focused on the uncertainty of the measurements of detailed response characteristics for identical structures subjected to the same impact conditions. Response characteristics such as pressure wall equivalent single hole diameter, pressure wall damage area, and rear-side spall area were analyzed to determine the level of uncertainty in the data generated using the test facility as well as the consistency of the damage levels found in dual-wall structures under hypervelocity impact.

IV. Repeatability Analysis Methodology

A review of the Phase B and Phase C/D impact test parameter databases revealed an unfortunate circumstance: very few of the impact tests were repeated under the same impact conditions. Thus, a traditional repeatability analysis of the phenomena involved in the response of dual-wall structures to hypervelocity projectile impact was impossible to perform. However, rather than abandon the entire exercise, a modified repeatability analysis was performed by pooling together several related groups of tests. This resulted in sample sizes of at least five–10 related tests per group. Though the pooled test groups were by no means large, some sort of comparison and assessment of phenomena repeatability became possible. For example, one such grouping was all tests performed on dual-wall structures without MLI and with a 1.6-mm-thick bumper, a 3.175-mm-thick pressure wall, and a 10.16-cm stand-off distance. Within that group, tests were then paired according to similarity in projectile diameter, trajectory obliquity, and impact velocity. The test pairs and groups used in the repeatability analysis can be found in Ref. 3.

Using the test pairs and groupings so created, a quantifiable level of repeatability for dual-wall systems tested in the NASA/MSFC light gas gun was determined by calculating the number of test pairs within a group of tests that did or did not sustain pressure wall perforation or rear-side spall in both tests of each test pair. The repeatability for that group of tests was then stated as the percentage of test pairs that were in agreement with regard to pressure wall perforation or rear-side spallation. This quantity will be referred to as the repeatability index for the specific group of tests under consideration. The results of the analyses performed for the various test groupings are summarized in Tables 2–6.

It may be noted that whereas Table 2 presents perforation and spallation repeatability indices for stand-off distances of 10.16, 15.24, and 30.48 cm, the results presented in Tables 3–6 are only for tests with a 10.16-cm stand-off distance. The small number of tests at the larger stand-off distances precluded any further detailed analyses. Finally, the entries 'N/A' in Tables 5a and 6 indicate the absence of any test pairs with the particular experimental parameter under consideration (i.e., impact velocity and bumper thickness in Tables 5a and 6, respectively).

V. Repeatability Analysis Results and Discussion

Results from the phenomena repeatability analysis presented in Tables 2–6 show that if three identical dual-wall structures with $t_w = 3.175$ mm and $S = 10.16$ cm were tested using the NASA/MSFC light gas gun under similar impact conditions (i.e., identical projectile diameter and trajectory

Table 2 Overview of perforation and spallation repeatability

Test group	BP/ BNP[a]	OP/ ONP[b]	PRI[c]	BS/ BNS[d]	OS/ ONS[e]	SRI[f]
$2.9 < V < 7.3$ km/s θ (deg) = 0, 45, 60, 65, 75 D (cm) = 0.475, 0.635, 0.795, 0.953 S (cm) = 10.16 t_s (mm) = 1.02, 1.27, 1.60, 2.03 With MLI	36	16	69.2%	46	6	88.5%
$5.1 < V < 6.9$ km/s θ (deg) = 0, 45 D (cm) = 0.635, 0.795, 0.953 S (cm) = 30.48 t_s (mm) = 1.6 With MLI	3	2	60.0%	2	3	40.0%
$3.6 < V < 7.2$ km/s θ (deg) = 0, 30 D (cm) = 0.475, 0.635, 0.795 S (cm) = 10.16 t_s (mm) = 1.60, 2.03 Without MLI	10	2	83.3%	12	0	100.0%
$3.7 < V < 7.1$ km/s θ (deg) = 0 D (cm) = 0.475, 0.635 S (cm) = 15.24 t_s (mm) = 1.6 Without MLI	4	3	57.1%	3	4	42.9%
Overall	53	23	69.7%	63	13	82.9%

[a]Both tests perforated or both tests not perforated.
[b]One test perforated and one test not perforated.
[c]Perforation repeatability index.
[d]Both tests spalled or both tests not spalled.
[e]One test spalled and one test not spalled.
[f]Spallation repeatability index.

obliquity, impact velocity within 0.2 km/s), then it is likely that either the pressure walls in two of these three tests will be perforated or will not be perforated. This is espcially true if the impact conditions (i.e., projectile diameter and velocity) are near those of the ballistic limit for the structure under consideration. These Tables also show that the repeatability of rear-side spallation (or the lack thereof) in such dual-wall structures is considerably higher: of ten tests performed, it is highly likely that nine of them will all either show some sort of rear-side spallation or nine of them will not. A more detailed review of Tables 2–6 reveals the following trends in perforation and spallation repeatability for dual-wall structures based on the Phase B and C/D impact testing performed using the NASA/MSFC gas gun.

A. Repeatability as a Function of Stand-Off Distance

Although the number of tests with a 10.16-cm stand-off distance was much greater than the number of tests with a stand-off distance larger than 10.16 cm, a certain trend is still discernable in the data presented in Table 2. It is apparent that the perforation and spallation repeatability indices for $S = 15.24$ and 30.48 cm are much lower than those for $S = 10.16$ cm. The most significant effect of increasing the stand-off distance on the response of a dual-wall structure is that a large stand-off distance allows significant expansion of the debris cloud created by the initial impact before it strikes the pressure wall plate. Thus, the debris cloud is more compact when $S = 10.16$ cm than when $S = 30.48$ cm. Any inhomogeneities in the debris cloud (e.g., pockets of air, solid particle concentrations, etc.) are likely to have a significant effect when the debris cloud is allowed to expand. Otherwise, when the debris cloud is relatively compact, debris cloud inhomogeneities are overwhelmed by the overall debris cloud loading. Thus, tests with $S = 30.48$ cm exhibit variations in response from test to test because of debris cloud inhomogeneities, which are a function of material defects and metallurgical imperfections, which also vary from test to test.

B. Repeatability as a Function of Multilayer Thermal Insulation Presence

In the limited instances where comparisons between perforation repeatability indices for structures with and without MLI were possible (i.e., in Table 3: $\theta = 0$ deg, 30 deg, in Table 4: $D = 0.635$ cm and $D = 0.795$, 0.953 cm, in Table 5b: $6 < V < 7$ km/s, and, in Table 6: $t_s = 1.6$ mm), it appears that the perforation repeatability indices for structures without MLI were greater than those for structures with MLI by approximately 23%. This increased perforation repeatability for dual-wall structures without MLI is probably due to the fact that adding the MLI introduced another variable into the impact process. This added variable would naturally affect the interaction of the various processes, increase the range of possible response characteristics, and therefore decrease the repeatability compared to systems in which MLI was not present.

C. Repeatability as a Function of Impact Angle

As the impact angle was increased from 0 to 75 deg, the repeatability indices for dual-wall structures with MLI decreased from 72% to 63% (Table 3). When the impact angle is below the critical angle of obliquity,[2] a majority of the material in the debris cloud is forced into the dual-wall system; only a small amount is expelled rearward as backsplash or ricochet debris. For impact angles exceeding the critical angle, a major-

Table 3 Perforation and spallation repeatability as a function of impact angle ($S = 10.16$ cm)

Test group	BP/ BNP	OP/ ONP	PRI	BS/ BNS	OS/ ONS	SRI
		$\theta = 0$ deg, 30 deg				
$0.9 < V < 7.3$ km/s D (cm) = 0.475, 0.635, 0.795, 0.953 t_s (mm) = 1.02, 1.60 With MLI	18	7	72.0%	23	2	92.0%
$3.6 < V < 7.2$ km/s D (cm) = 0.475, 0.635, 0.795 t_s (mm) = 1.60, 2.03 Without MLI	7	2	77.8%	9	0	100.0%
		$\theta = 45$ deg				
$3.1 < V < 6.9$ km/s D (cm) = 0.475, 0.635, 0.953 t_s (mm) = 1.27, 2.03 With MLI	13	6	72.2%	16	3	88.9%
$6.6 < V < 7.0$ km/s D (cm) = 0.635, 0.795 t_s (mm) = 1.60 Without MLI	2	0	(1)[a]	2	0	(1)[a]
		$\theta = 60$ deg, 65 deg, 75 deg				
$2.9 < V < 6.5$ km/s D (cm) = 0.635, 0.795 t_s (mm) = 1.02, 1.27, 2.03 With MLI	5	3	63.5%	8	0	100.0%
$7.1 < V < 7.3$ km/s D (cm) = 0.475 t_s (mm) = 1.60 Without MLI	1	0	(1)	1	0	(1)
Overall	46	18	71.9%	59	5	92.2%

[a]Sufficient number of tests not available for repeatability index calculation.

ity of the debris cloud material is expelled as ricochet debris. For aluminum projectile impacting thin aluminum plates, this critical angle of impact has been shown to be approximately 60–65 deg.[2] Thus tests performed near the critical angle (i.e., at 60 deg and 65 deg) may show a wide variation in response characteristics as the response of the dual-wall system makes a transition from one mode of response (inward traveling debris clouds) to another (outward traveling or ricochet debris clouds).

D. Repeatability as a Function of Projectile Diameter

Both the perforation and the spallation repeatability indices increased with projectile diameter as shown in Table 4. This may be explained by the fact that the larger projectiles were deformed less in their flights through the light gas gun than were the smaller diameter projectiles. This in-flight projectile deformation for the smaller projectiles naturally affected the orientation of the smaller projectiles at impact which significantly affected the consistency of system response in such cases.

E. Repeatability as a Function of Impact Velocity

As can be seen in Tables 5a and 5b, the perforation repeatability index varies from 90% at impact velocities below 4 km/s to 57% for velocities between 5–6 km/s, and back again to 90% for speeds in excess of 7 km/s. For aluminum-on-aluminum impacts, below a velocity of approximately 4 km/s, pressure wall perforation is driven by mechanical processes such as fracture. These processes are very sensitive to mechanical or metallurgical imperfections so that in low-velocity impacts the repeatability of pressure wall perforation will be dependent on metallurgical consistency of the test specimen from test to test. If such consistency is not maintained, perforation repeatability in relatively low-velocity impacts will be relatively low. It is noted that when the impact velocity is low enough so that perforation of the pressure wall is not likely to occur, we can expect repeatability to go up again because the response (i.e., nonperforation) will be more consistent. Alternatively, for impact velocities above approximately 6.5 km/s, pressure wall perforation is driven by hydrodynamical considerations which are not as sensitive to mechanical defects as mechanical processes such as fracture. In such cases, the response is expected to be relatively uniform.

Table 4 Perforation and spallation repeatability as a function of projectile diameter (S = 10.16 cm)

Test group	BP/ BNP	OP/ ONP	PRI	BS/ BNS	OS/ ONS	SRI
D = 0.475 cm 6.4< V <7.3 km/s θ (deg) = 0, 45 t_s (mm) = 1.02, 2.03 With MLI	1	1	(1)	2	0	(1)
3.6< V <7.3 km/s θ (deg) = 0, 65 t_s (mm) = 1.60, 2.03 Without MLI	2	1	66.7%	3	0	100.0%
D = 0.635 cm 2.9< V <6.9 km/s θ (deg) = 0, 45, 65 t_s (mm) = 1.02, 1.27, 1.60, 2.03 With MLI	16	10	61.5%	21	5	76.9%
4.9< V <7.2 km/s θ (deg) = 0, 30, 45 t_s (mm) = 1.60 Without MLI	4	1	80.0%	5	0	100.0%
D = 0.795, 0.953 cm 2.9< V <7.2 km/s θ (deg) = 0, 45, 60, 75 t_s (mm) = 1.02, 1.27, 1.60, 2.03 With MLI	19	5	79.2%	24	0	100.0%
4.3< V <6.8 km/s θ (deg) = 0, 45 t_s (mm) = 1.60 Without MLI	4	0	100.0%	4	0	100.0%
Overall	46	18	71.9%	59	5	92.2%

Table 5a Perforation and spallation repeatability as a function of impact velocity (S = 10.16 cm, 2.9< V <6 km/s)

Test group	BP/ BNP	OP/ ONP	PRI	BS/ BNS	OS/ ONS	SRI
2.9< V <4 km/s θ (deg) = 0, 45, 75 D (cm) = 0.635, 0.795 t_s (mm) = 1.60, 2.03 With MLI	9	1	90.0%	9	1	90.0%
θ (deg) = 0 D (cm) = 0.475 t_s (mm) = 2.03 Without MLI	0	1	(1)	1	0	(1)
4< V <5 km/s θ (deg) = 0, 65 D (cm) = 0.635 t_s (mm) = 1.60 With MLI	1	1	(1)	1	1	(1)
θ (deg) = 0 D (cm) = 0.475, 0.635, 0.795 t_s (mm) = 1.60, 2.03 Without MLI	3	0	100.0%	3	0	100.0%
5< V <6 km/s θ (deg) = 45 D (cm) = 0.635 t_s (mm) = 1.27 With MLI	4	3	57.1%	4	3	57.1%
Without MLI	N/A	N/A	N/A	N/A	N/A	N/A

Table 5b Perforation and spallation repeatability as a function of impact velocity (S = 10.16 cm, 6< V <8 km/s)

Test group	BP/ BNP	OP/ ONP	PRI	BS/ BNS	OS/ ONS	SRI
6< V <7 km/s θ (deg) = 0, 45, 75 D (cm) = 0.475, 0.635, 0.795, 0.953 t_s (mm) = 1.02, 1.27, 1.60, 2.03 With MLI	15	10	60.0%	24	0	100.0%
θ (deg) = 0, 30, 45 D (cm) = 0.635, 0.795 t_s (mm) = 1.60 Without MLI	5	1	83.3%	6	0	100.0%
7< V <8 km/s θ (deg) = 0 D (cm) = 0.475, 0.795 t_s (mm) = 1.02, 1.60 With MLI	7	1	87.5%	9	0	100.0%
θ (deg) = 30, 65 D (cm) = 0.475, 0.635 t_s (mm) = 1.60 Without MLI	2	0	(1)	2	0	(1)
Overall[a]	46	18	71.9%	49	5	92.2%

[a]Includes Tables 5a and 5b.

F. Repeatability as Function of Bumper Thickness

From Table 6, it can be seen that the perforation repeatability index increases from 50% for t_s = 1.02 mm to 80% for t_s = 2.03 mm for dual-wall structures with MLI. The lack of

Table 6 Perforation and spallation repeatability as a function of bumper thickness (S = 10.16 cm)

Test group	BP/ BNP	OP/ ONP	PRI	BS/ BNS	OS/ ONS	SRI
t_s = 1.02 mm 4.6< V <7.3 km/s D (cm) = 0.475, 0.635, 0.795 θ (deg) = 0, 65 With MLI	3	3	50.0%	6	0	100.0%
Without MLI	N/A	N/A	N/A	N/A	N/A	N/A
t_s = 1.27 mm 2.9< V <6.4 km/s D (cm) = 0.635, 0.953 θ (deg) = 45, 60 With MLI	8	7	53.3%	12	3	80.0%
Without MLI	N/A	N/A	N/A	N/A	N/A	N/A
t_s = 1.60 mm 2.9< V <7.2 km/s D (cm) = 0.635, 0.795, 0.953 θ (deg) = 0 With MLI	17	4	80.9%	19	2	90.4%
4.3< V <7.3 km/s D (cm) = 0.475, 0.635, 0.795 θ (deg) = 0, 30, 45, 65 Without MLI	9	1	90.0%	10	0	100.0%
t_s = 2.03 mm 3.1< V <6.9 km/s D (cm) = 0.475, 0.635, 0.795 θ (deg) = 45, 75 With MLI	8	2	80.0%	10	0	100.0%
3.6< V <4.3 km/s D (cm) = 0.475 θ (deg) = 0 Without MLI	1	1	(1)	2	0	(1)
Overall	46	18	71.9%	59	5	92.2%

sufficient data for structures without MLI except in one test group prevents any conclusions from being drawn regarding the effect of bumper thickness on repeatability for such structures. With regard to spallation for dual-wall structures with MLI, the repeatability index starts out to be quite high for very thin bumper plates, decreases slightly as the bumper thickness increases, and then increases to a high level for the thickest bumper plate. Because MLI is present in these dual-wall systems, the agreement is found with respect to the nonoccurrence of rear-side spall; the spall that did occur in the tests with medium-thickness bumper plates was minimal. Therefore, the variation in the repeatability index for rear-side spall as a function of bumper thickness is not very significant.

VI. Uncertainty Analysis Methodology

The second stage of the analysis consists of a more traditional uncertainty analysis of the experimental data obtained from the high-speed impact tests. These methods were somewhat modified to account for the paucity of tests under identical test conditions. In addition, two different but related approaches were used in performing the uncertainty analyses. Because of the scarcity of tests with the same impact parameters, it was not possible to determine the uncertainty in actual test results for bumper plate hole diameter, for example, or for pressure wall damage area. However, by pooling together the results of several related tests, it became possible to determine the uncertainty in the ratios of, for example, pressure wall damage area for all the pairs of tests within a specific group.

The first approach was based on the presumption that the lack of sufficient information precluded making any specific comments regarding the true value of any parameter based on the experimental data available. However, in this case, it was still possible to calculate for a given confidence level c and for the parameters of the test group under consideration, the interval within which c% of the response parameter ratios would be expected to fall if more tests were performed under similar impact conditions. These results can also be used to state that there would be a c% probability that a test ratio pair would lie in the calculated response parameter ratio interval.

The second approach differs from the first in that it was used to calculate, for a given confidence level c and for the parameters of the test group under consideration, the interval within which it can be supposed lay the true value of a damage response parameter for a given set of impact parameters relative to test data obtained at those same parameters. In both approaches, the calculations performed assumed that there were no bias errors present in the data. These two approaches are discussed in more detail in Secs. VI.A and VI.B, respectively.

A. Uncertainty Analysis—First Approach

Mathematically, a c% response parameter ratio interval can be defined as follows:

$$\mu_\rho - \eta_c \sigma_\rho < \rho < \mu_\rho + \eta_c \sigma_\rho \tag{1}$$

where μ_ρ and σ_ρ are the mean and standard deviations of the ratios ρ for a particular quantity (i.e., hole diameter, damage area, etc.) for the test pairs within a specific test group. The quantity η_c is a numerical multiplier that is obtained from statistical tables (see, e.g., Refs. 4 and 5) and is a function of the number of ratios considered in calculating μ_ρ and σ_ρ and the level of confidence c specified.

It should be noted here that there are two basic ways of calculating the ratios described here. The first is to force all the ratios within a test group to be less than unity by dividing the smaller of the two quantities in the test pairs by the larger; the second is to force all the ratios within a test group to be greater than unity by doing the exact opposite. Because there is no reason to suppose that the next response parameter ratio will be less than or greater than one, it may be argued that the appropriate interval to be calculated for a given confidence level is given by

$$\mu_{\rho<1} - \eta_c \sigma_{\rho<1} < \rho_o < \mu_{\rho>1} + \eta_c \sigma_{\rho>1} \tag{2}$$

where $\mu_{\rho<1}$ and $\sigma_{\rho<1}$ are the mean and standard deviation of the ratios for a particular response quantity, respectively, when all the ratios are less than one, and $\mu_{\rho>1}$ and $\sigma_{\rho>1}$ are the mean and standard deviation of the ratios for a particular response quantity, respectively, when all the ratios are greater than one. In Eq. (2), ρ_o represents the ratio of two response parameter values without any specification that the ratio be less than or greater than one. It is this modified c% confidence interval that will be used to specify the range within which c% of the response parameter ratios would be expected to fall if a large number of tests were performed under similar test conditions.

The analyses described in the previous paragraphs require the assumption of a certain confidence level c to determine a modified c% confidence interval. The specified value of c and the number of degrees of freedom n in a particular test group (which equals one less than the number of tests N within a specific group) is the information required to obtain the appropriate value of η_c to be used in Eq. (3). Values of η_c for certain values of c and $n = N - 1$ are given in Table 7; Tables 8–10 contain mean and standard deviation values for the various test groupings considered in this part of the study.

B. Uncertainty Analysis—Second Approach

The equations required for the second approach are obtained using the same principles as those which were used in

Table 7 Values of η_c as a function of number of degrees of freedom (n) and confidence level (c)[5]

	c							
n	0.60	0.75	0.90	0.95	0.975	0.99	0.995	0.9995
1	0.325	1.000	3.078	6.314	12.706	31.821	63.657	636.619
2	0.289	0.816	1.886	2.920	4.303	6.965	9.925	31.598
3	0.277	0.765	1.638	2.353	3.182	4.541	5.841	12.924
4	0.271	0.741	1.533	2.132	2.776	3.747	4.604	8.610
5	0.267	0.727	1.476	2.015	2.571	3.365	4.032	6.869
6	0.265	0.718	1.440	1.943	2.447	3.143	3.707	5.959
7	0.263	0.711	1.415	1.895	2.365	2.998	3.499	5.408
8	0.262	0.706	1.397	1.860	2.306	2.896	3.355	5.041
9	0.261	0.703	1.383	1.833	2.262	2.821	3.250	4.781
10	0.260	0.700	1.372	1.812	2.228	2.764	3.169	4.587
11	0.260	0.697	1.363	1.796	2.201	2.718	3.106	4.437
12	0.259	0.695	1.356	1.782	2.179	2.681	3.055	4.318
13	0.259	0.694	1.350	1.771	2.160	2.650	3.012	4.221
14	0.258	0.692	1.345	1.761	2.145	2.624	2.977	4.140
15	0.258	0.691	1.341	1.753	2.131	2.602	2.947	4.073
16	0.258	0.690	1.337	1.746	2.120	2.583	2.921	4.015
17	0.257	0.689	1.333	1.740	2.110	2.567	2.898	3.965
18	0.257	0.688	1.330	1.734	2.101	2.552	2.878	3.922
19	0.257	0.688	1.328	1.729	2.093	2.539	2.861	3.883
20	0.257	0.687	1.325	1.725	2.086	2.528	2.845	3.850
21	0.257	0.686	1.323	1.721	2.080	2.518	2.831	3.819
22	0.256	0.686	1.321	1.717	2.074	2.508	2.819	3.792
23	0.256	0.685	1.319	1.714	2.069	2.500	2.807	3.767
24	0.256	0.685	1.318	1.711	2.064	2.492	2.797	3.745
25	0.256	0.684	1.316	1.708	2.060	2.485	2.787	3.725
26	0.256	0.684	1.315	1.706	2.056	2.479	2.779	3.707
27	0.256	0.684	1.314	1.703	2.052	2.473	2.771	3.690
28	0.256	0.683	1.313	1.701	2.048	2.467	2.763	3.674
29	0.256	0.683	1.311	1.699	2.045	2.462	2.756	3.659
30	0.256	0.683	1.310	1.697	2.042	2.457	2.750	3.646
40	0.255	0.681	1.303	1.684	2.021	2.423	2.704	3.551
60	0.254	0.679	1.296	1.671	2.000	2.390	2.660	3.460
120	0.254	0.677	1.289	1.658	1.980	2.358	2.617	3.373
∞	0.253	0.674	1.282	1.645	1.960	2.326	2.576	3.291

Table 8 Bumper plate hole diameter ratio uncertainty data

θ (deg)	N	$\mu_{\rho<1}$	$\sigma_{\rho<1}$	$\mu_{\rho>1}$	$\sigma_{\rho>1}$
0	20	0.944	0.050	1.062	0.058
45	18	0.940	0.060	1.068	0.074
		0.953	0.036	1.051	0.040
60, 65, 75	9	0.937	0.055	1.070	0.067
		0.937	0.049	1.070	0.058

the derivation of the equations for the first approach. As before, since we do not know if the true value of a response parameter under consideration is less than or greater than an existing (or a future) test value, it can be argued that a modified c% confidence interval may be written as

$$\mu_{\rho<1} - \eta_c \sigma_{\rho<1} < \rho_o < \mu_{\rho>1} + \eta_c \sigma_{\rho>1} \tag{3}$$

where in this case ρ_o represents the ratio of the true value to a test value without any specification that the ratio be less than or greater than one. Values for η_c are again found using Table 7 and, as before, Tables 8–10 are used to obtain mean and standard deviation values for the various test groupings considered.

VII. Uncertainty Analysis Results and Discussion

This section consists of a discussion of the results obtained using the two approaches to the data uncertainty analysis developed in Sec. VI. Also presented are several examples using the equations derived and the information provided in Tables 7–10. The use of the tables and equations for the two approaches is demonstrated first, followed by a discussion of the observable trends in the uncertainty analysis data. It is noted that in Table 8, for a nonzero impact angle, the first and second lines of information pertain to the minimum and maximum hole dimensions, respectively.

A. Illustrative Examples—First Approach

The data in Tables 7–10 can be used to calculate intervals within which a certain percentage of response parameter ratios can be expected to lie, given a certain level of confidence. Alternatively, the specified confidence level is the probability

Table 9 Pressure wall hole diameter ratio uncertainty data

	MLI	N	$\mu_{\rho<1}$	$\sigma_{\rho<1}$	$\mu_{\rho>1}$	$\sigma_{\rho>1}$
	As a function of impact angle θ (deg)					
$\theta = 0$	Y	11	0.855	0.117	1.152	0.185
	N	5	0.723	0.147	1.439	0.343
$\theta = 45$	Y	7	0.698	0.250	1.616	0.613
	N	—	—	—	—	—
	As a function of bumper thickness t_s (mm)					
$t_s = 1.27$	Y	4	0.601	0.272	1.887	0.675
	N	—	—	—	—	—
$t_s = 2.03$	Y	3	0.827	0.181	1.253	0.305
	N	—	—	—	—	—
	As a function of impact velocity V (km/s)					
$3 < V < 5.5$	Y	5	0.854	0.093	1.184	0.150
	N	2	0.822	0.038	1.218	0.056
$5.5 < V < 8$	Y	13	0.712	0.301	1.398	0.150
	N	3	0.656	0.162	1.586	0.391
	As a function of projectile diameter D (cm)					
$D = 0.635$	Y	8	0.735	0.235	1.522	0.592
	N	2	0.837	0.017	1.195	0.024
$D = 0.795$	Y	8	0.646	0.146	1.169	0.221
	N	3	0.876	0.123	1.601	0.369

Table 10 Pressure wall damage area ratio uncertainty data

	MLI	N	$\mu_{\rho<1}$	$\sigma_{\rho<1}$	$\mu_{\rho>1}$	$\sigma_{\rho>1}$
	As a function of impact angle θ (deg)					
$\theta = 0$	Y	21	0.746	0.223	1.510	0.610
	N	8	0.735	0.172	1.448	0.442
$\theta = 45$	Y	18	0.864	0.092	1.170	0.135
	N	—	—	—	—	—
$\theta = 60$, 65, 75	Y	8	0.571	0.181	1.953	0.762
	N	—	—	—	—	—
	As a function of bumper thickness t_s (mm)					
$t_s = 1.02$	Y	6	0.610	0.240	1.864	0.699
	N	—	—	—	—	—
$t_s = 1.27$	Y	14	0.777	0.277	1.280	0.367
	N	—	—	—	—	—
$t_s = 1.60$	Y	16	0.784	0.192	1.388	0.570
	N	8	0.689	0.166	1.534	0.399
$t_s = 2.03$	Y	10	0.739	0.166	1.452	0.517
	N	—	—	—	—	—
	As a function of impact velocity V (km/s)					
$3 < V < 5.5$	Y	12	0.776	0.226	1.448	0.612
	N	4	0.568	0.451	1.456	0.649
$5.5 < V < 8$	Y	34	0.763	0.185	1.442	0.490
	N	6	0.677	0.114	1.518	0.299
	As a function of projectile diameter D (cm)					
$D = 0.475$	Y	—	—	—	—	—
	N	3	0.520	0.345	2.552	1.519
$D = 0.635$	Y	25	0.803	0.181	1.338	0.432
	N	4	0.664	0.147	1.577	0.423
$D = 0.795$	Y	18	0.725	0.194	1.514	0.555
	N	4	0.714	0.202	1.489	0.430

that a particular response parameter ratio is within the calculated interval. In either case, it is assumed that there is no fixed or bias error present in the experimental readings.

As an example, consider a test series in which 0.795-cm-diam projectiles normally impact a dual-wall system at a speed of 6.5 km/s. We wish to know the extents of the intervals within which 75% and 90% of the bumper plate hole diameter ratios lie for the given impact conditions. Using Eq. (2) together with the values of $\mu_{\rho<1}$, $\sigma_{\rho<1}$ and $\mu_{\rho>1}$, $\sigma_{\rho>1}$ in Table 8 for a 0-deg impact, we have

$$0.944 - 0.050\eta_c < \rho_o < 1.062 + 0.058\eta_c \tag{4}$$

where η_c is dependent on the specified confidence level c and the number of degrees of freedom $n = N - 1$ in the test group under consideration. In this case, $N = 20$ so that $n = 19$; if we specify a 75% confidence level, then from Table 7 we see that $\eta_c = 0.688$. Substituting $\eta_c = 0.688$ into Eq. (4) indicates that there is a 75% probability that, if fixed errors in data collection are ignored, the ratio of the bumper plate hole diameters for two additional tests at similar impact conditions will lie between 0.906 and 1.102.

For a 90% confidence level, Table 7 tells us that $\eta_c = 1.328$. Substituting this value into Eq. (4) results in an interval that extends from 0.878 to 1.139. In this case, as for the previous confidence level considered, the range of the interval about unity is relatively small (only 10–12% on either side of unity). This is due to the small deviations of the ratios of recorded hole diameter ratios about a value of 1.0 as is evidenced by the proximity of the means $\mu_{\rho<1}$ and $\mu_{\rho>1}$ to 1.0 and the small values of the standard deviations $\sigma_{\rho<1}$ and $\sigma_{\rho>1}$ in Table 8.

The same procedure can be used to determine modified confidence intervals for pressure wall hole diameter data in the event of a perforation. For example, for a test series using dual-wall systems with MLI at $V = 6.5$ km/s where pressure wall perforation does occur, Eq. (2) and the information in Table 9 yields

$$0.712 - 0.301\eta_c < \rho_o < 1.398 + 0.150\eta_c \tag{5}$$

For a 75% confidence level with, in this case, $n = 13 - 1 = 12$, Table 7 provides a value of $\eta_c = 0.695$. Thus, the 75% modified confidence interval for a test series under these conditions extends from 0.503 to 1.502. In turn, this tells us that there is a 75% probability that in the two tests in which perforation had occurred, the ratio between the pressure wall hole diameters will lie between 0.503 and 1.502. As can be seen from this example, the extent of the modified confidence interval for the pressure wall hole diameter data is significantly larger than that for the bumper plate hole diameter data for the same level of confidence.

B. Illustrative Examples—Second Approach

The data in Tables 7–10 can also be used to calculate intervals within which it may be supposed that the true value of a response parameter lies, given a certain level of confidence. Alternatively, the specified confidence level is the probability that the supposedly true value of a response parameter is within the calculated interval. In either case, as before, it is assumed that there is no fixed or bias error present in the experimental readings.

As an example, consider a test in which a 0.795-cm-diam projectile normally impacted a dual-wall system at a speed of 6.55 km/s. The recorded diameter of the hole in the bumper plate is 1.636 cm.[3] We wish to know how representative of the actual or true bumper plate hole diameter is the recorded value for the given impact conditions. Using Eq. (3) and the values of $\mu_{\rho<1}$, $\sigma_{\rho<1}$ and $\mu_{\rho>1}$, $\sigma_{\rho>1}$ in Table 8 for a 0-deg impact, we arrive at Eq. (4), which provides the interval within which the true value of hole diameter for the given conditions can be expected to be. As before, for a 75% confidence level, Table 7 again yields $\eta_c = 0.688$. Substituting $\eta_c = 0.688$ into Eq. (4) suggests that there is a 75% probability that, if fixed errors in data collection are ignored, the actual or true value of the bumper hole diameter lies between 0.906 and 1.102 times the recorded value, or between 1.481 and 1.801 cm. For a 90% confidence level, similar calculations indicate that the interval extends from 1.435 to 1.864 cm.

C. Observations on the Data

As can be seen by inspecting the mean and standard deviation values in for the various test groups in Tables 8–10, the level of uncertainty in the response data can vary significantly depending on the response parameter considered. Specifically, because the means of the bumper plate diameter data are all fairly close to 1.0 and the standard deviations are all fairly small (Table 8), we can be confident that the recorded values of the bumper plate hole diameter are consistent and may indeed be representative of the actual or true hole diameter values. However, this is not necessarily the case for the pressure wall hole diameter or pressure wall damage area values. The means and standard deviation values in Tables 9 and 10 indicate that there can be a significant amount of uncertainty in the pressure wall response data.

While the information presented in Tables 8–10 has been used thus far to assess uncertainty in impact test data, it can also be used for drawing other related conclusions. Specifically, the data in Tables 8–10 provides insight into the sensitivity of dual-wall system response to minute differences in impact conditions, material composition, specimen thickness, etc, for example, if we consider a response parameter, such as bumper plate hole diameter, whose modified confidence interval is relatively small (e.g., ± 10%) at a relatively high confidence level (e.g., 90%). In this case, it can be said that the parameter is relatively insensitive to small changes such as those listed in the previous paragraph, and that the data for this parameter are expected to be consistent from one test to another, despite the fact that there may be small unavoidable differences present. This in turn implies that a relatively small number of tests will be required to characterize such a parameter under the test conditions of interest.

Alternatively, for a response parameter such as pressure wall damage area, whose modified confidence interval is relatively large (e.g., ± 50%) even at relatively low confidence levels (e.g., 75%), it may be argued that the parameter is in fact highly sensitive to minute changes in test conditions. The data for this parameter are highly scattered and are not expected to be consistent from one test to another. For such a response parameter, small unavoidable variations from test to test will apparently result in differences in response which will in turn result in the scatter of the test data. This in turn implies that a relatively large number of tests will be required to characterize such a response parameter under the test conditions of interest.

It should also be noted that the observed variations in perforation and rear-side spallation response characteristics are probably not due to an inability to properly control the experimental parameters of the tests performed. Geometric parameters (thicknesses and wall-to-wall spacing), material properties (density, modulus, etc.) and impact conditions (diameter, angle, and velocity) can all be controlled to within acceptable tolerances. The variations observed are probably due to factors that to date have not been measured, accounted for, or controlled. Such factors include manufacturing defects, metallurgical inconsistencies, and location of the initial impact on the bumper plate, to name a few. These and any other factors must be considered to improve the repeatability of the phenomena observed through hypervelocity impact testing using the NASA/MSFC light gas gun.

VIII. Conclusions and Recommendations

Phenomena repeatability and data uncertainty analyses were performed using the data generated using the NASA/MSFC high-speed impact test facility as part of the Space Station Phase B and Phase C/D development test efforts. The

analyses sought to quantify the repeatability of the phenomena occurring in dual-wall structures under hypervelocity impact based on the testing performed using the NASA/MSFC light gas gun during the time period of 1985–1991 and to determine the uncertainty of the measurments taken from damaged test specimens.

The results of the phenomena repeatability analysis show that if three identical dual-wall structures were to be tested using the NASA/MSFC light gas gun under similar impact conditions, then it is entirely likely that either the pressure walls in two of these three tests will be perforated and one will not, or the pressure walls in two of these tests will not be perforated and one will. The results obtained also show that the repeatability of rear-side spallation (or the lack thereof) in such dual-wall structures is considerably higher: of ten tests performed, it is highly likely that nine of them will all either show some sort of rear-side spallation and one will not or nine of them will not be spalled and one of them will. The results of the uncertainty analysis show that the level of uncertainty in the response data can vary significantly depending on the response considered. However, the observations made in the uncertainty analysis in general reinforce those made during the repeatability analysis. The results of both phases of the analysis indicate that repeatability and consistency in response characteristics increase as the impact angle decreases, the projectile diameter increases, and as the bumper thickness increases.

Acknowledgments

The authors are grateful for the support from the NASA/MSFC under contract NAS8-36955/DO74. The authors would like to acknowledge the assistance provided by the NASA/MSFC Technical Contracting Officer, Miria Finckenor (Engineering Physics Division, Physical Sciences Branch). The authors would also like to express their appreciation to Jim Zweiner, Roy Taylor (ret.), Hubert Smith (ret.), and Joe Lambert (ret.) of the NASA/MSFC Laboratory Support Branch, Phillip Petty and Robert Stowell of the Martin Marietta Corporation, and Mike Bjorkman, Ben Ramsey, and Earl Shirley of the Boeing Corporation for conducting the impact testing that made this investigation possible. Finally, the authors would like to express their gratitude to Hugh Coleman, Professor of Mechanical and Aerospace Engineering at the University of Alabama in Huntsville for his advice on matters pertaining to experimental repeatability analysis.

References

[1]Taylor, R. A., "A Space Debris Simulation Facility for Spacecraft Materials Evaluation," *SAMPE Quarterly,* Vol. 18, No. 2, 1987, pp. 28–34.

[2]Schonberg, W. P., Bean, A. J., and Darzi, K., *Hypervelocity Impact Physics,* NASA CR-4343, Final Rept., Contract NAS8-36955/DO16, Jan. 1991.

[3]Schonberg, W. P., and Cooper, D., *Repeatability and Uncertainty Analyses of NASA/MSFC Light Gas Gun Test Data,* Final Rept., Contract NAS8-36955/DO74, March, 1993.

[4]Coleman, H. W., and Steele, W. G., *Experimentation and Uncertainty Analysis for Engineers,* John Wiley, New York, 1989.

[5]Fisher, R. A., and Yates, F., *Statistical Tables,* Oliver and Boyd, Ltd., London, 1938.